Revision 3

The Bi sulfates from the Alfenza Mine, Crodo, Italy: An Automatic Electron Diffraction Tomography (ADT) Study

Gian Carlo Capitani[1,]*, Enrico Mugnaioli[2], Jordi Rius[3], Paolo Gentile[1],
Tiziano Catelani[4], Andrea Lucotti[5], and Ute Kolb[2,6]

[1]Dipartimento di Scienze dell'Ambiente e del Territorio e di Scienze della Terra, Università degli Studi di Milano-Bicocca, Milano, Italy.
[2]Institute of Physical Chemistry, Johannes Gutenberg University, Mainz, Germany.
[3]Institute of Materials Science of Barcelona (CSIC), Barcelona, Catalonia, Spain.
[4]Dipartimento di Scienze della Terra, Università degli Studi di Firenze, Firenze, Italy.
[5]Dipartimento di Chimica, Materiali ed Ingegneria Chimica "G. Natta", Politecnico di Milano, Milano, Italy.
[6]Institute of Applied Geosciences, Darmstadt University of Technology, Darmstadt, Germany.

*Corresponding author: giancarlo.capitani@unimib.it

Abstract

We report about three bismuth sulfates from mineralized quartz dikes from Alfenza (Crodo, Italy), two new phases and a rare mineral, cannonite, all growing on bismuthinite. The first new phase occurs as white, "hortensia-like" aggregates of pseudo-hexagonal platelets, with perfect basal cleavage, ~20 micron wide and few microns thick. The approximate composition is $Bi_2O_2(SO_4)$, and cell parameters and symmetry, as determined by automatic diffraction tomography, are a = 22.0(4), b = 16.7(3), c = 15.9(3) Å, β = 102.9(5)°, space group Pc or $P2/c$. A major stacking disorder is detected by HR-SEM images and electron diffraction data.

The second new phase was detected only by TEM. It can be distinguished by its random orientation on the TEM grid (i.e., absence of preferential parting), the higher resistance under the electron beam, and different cell parameters and structure, whereas the composition is similar (Bi/S ~ 2.2/1), apart for the presence of tellurium up to ~6 cations %. The unit cell is hexagonal, space group $P\overline{6}2c$, a = 9.5(2) and c = 15.4(3) Å. In this case, a structure model was obtained *ab initio* from electron diffraction data. Interestingly, the mineral has a porous structure with one dimensional porosity (diameter of the channel ~7 Å).

Finally, within the same centimeter sized hand-specimens, we detected also cannonite. Its identification was done by automatic diffraction tomography. The measured cell parameters are a = 7.7(2), b = 13.9(3), c = 5.7(1) Å, β = 109.8(5)°, the space group $P2_1/c$. Cannonite at Alfenza forms radiating, acicular aggregates of colorless, transparent crystals with “scalpel-like” habit, elongated along **c**, up to 200 micron in length.

Introduction

Many natural and synthetic materials crystallize in grains not large enough or sufficiently ordered for conventional single crystal X-ray structural analysis, or not in sufficiently large amounts for powder X-ray diffraction. The latter, moreover, suffers of peaks superposition problems that limit any *ab initio* structure solution. Synchrotron radiation X-ray micro diffraction can be applied to this kind of materials, but its application nevertheless is very problematic since the very limited beamtime available at synchrotron facilities. Electron crystallography may be the solution to such cases, since crystallographic information can be extracted from nanosized volumes of material thanks to the strong electron-matter interaction, 10^3-10^4 times stronger than for X-rays. However, the strong electron-matter interaction is at the same time the main drawback of electron diffraction, since it causes multiple scattering, which makes the mathematical treatment of the diffraction process difficult. Because of this limitation, electron crystallography has never turned into a routine technique for crystal structure solution.

Things seem to take a different trend since the recent advent of the automatic electron diffraction tomography (ADT). This is a transmission electron microscopy (TEM) technique working similarly to an area detector single crystal X-ray diffractometer: the reciprocal space is explored and sampled rotating the crystal around an arbitrary axis and image frames are acquired every degree and integrated alike X-rays intensities. Working out of zone axis orientation, the dynamical nature of the electron diffraction is significantly reduced. Moreover, ADT can be combined with the Precession Electron Diffraction (PED), in which the electron beam is precessed around the optical axis of the microscope – a descan operation below the sample allows a stationary view of the electron diffraction pattern – with the net result that only a limited number of reciprocal nods are excited at a time, further reducing the dynamical effects (Vincent and Midgley 1994, Avilov et al. 2007). Finally, sample recognition and centering are performed in scanning (STEM) mode, thus reducing the electron dose at the sample and allowing the study of beam sensitive materials as those investigated in these study. A full description of the ADT technique can be found in Kolb et al. (2007, 2011) and Mugnaioli et al. (2009).

The samples described in this work come from mineralized quartz dikes intruding along fractures oriented NWW-SSE Triassic garnet micaschist, partially covered by tillitic deposits, and outcropping roughly one kilometer and two hundred meters from the confluence of the Alfenza stream with the Toce River, seven hundred meters NW from Crodo (Antigorio Valley, Ossola, Italy). The ore mineralogy mostly consists of pyrite, lesser arsenopyrite, bismuthinite and cosalite, and sporadic bornite, and was originated by mesothermal fluids after the main stages of the alpine orogenesis (Stella1943). From a geological point of view, this area represents a “Mesozoic window” within the Lepontine nappes, traditionally assigned to the ancient northern Penninic margin overthrusted during the continental collision of the alpine orogenesis by the oceanic lithosphere and the southern austroalpine margin, and in addition to the micaschist mentioned above, consists of pre-Triassic orthogneiss, Mesozoic mudstones and calceschists (Fig. 1).

The mineralized quartz dikes of Alfenza captured the attention of local traders probably ever since the XVII century due to their auriferous pyrite. The Alfenza mineralization is just one of the various auriferous manifestations present in the Ossola region, which has been the most renowned region in Italy for the exploitation of gold. After several periods of exploitation followed by stops, the Mine was definitely abandoned in 1941 (Roggiani 1948, 1970; Pipino 2003). What remains for the satisfaction of the mineralogists and of the mineral collectors is the rich variety of minerals that the Alfenza mince has furnished, including perfect crystals of bismuthinite (Bianchi 1924; Roggiani 1940) the sulfosalt cosalite (Ferraris et al. 1970), and native gold (Roggiani 1970). For a complete list of Alfenza's minerals see Roggiani (1946). In this respect, our contribution is about the discovery of new and rare (cannonite) bismuth sulfates that occur all together within the same centimeter sized samples, often within the same millimeter sized geodes, and form micrometers sized crystals with different appearances. These sulfates most probably originated from weathering and oxidization of pre-existing bismuthinite, that in these samples forms acicular, prismatic crystals up to several millimeters long, occurring in fan-shaped and interlaced aggregates, and represent the most abundant mineral after quartz. Other identified minerals sometimes present are pyrite, anglesite, micas and sporadic cosalite.

Experimental methods

SEM investigations were performed at the University of Milano Bicocca with a Tescan VEGA TS 5136XM. The low vacuum capability of the Tescan allows observations on rock fragments without a preliminary preparation, including carbon coating. Semiquantitative EDS analyses were performed on selected crystal fragments dispersed via ethanol on a glass section to favor the horizontal orientation of cleavage surfaces. Natural bismuthinite, anglesite and galena were used as standard. Standard sample preparation via epoxy embedding and polishing gave comparatively less reproducible results, probably because of fine scale intergrowths of several different phases, not resolvable in the BSE images. Similarly, wave dispersive microprobe analyses (WDS) probably caused damage to the sample and gave worse results because of the higher current employed in comparison to EDS (5 nA vs. 190 pA). High resolution SEM images were acquired at the University of Mainz with a FEI Nova NanoSEM 630 equipped with a field emission gun (FEG) source and a vCD backscatter detector (low-voltage, high-contrast detector).

Conventional TEM analyses were performed at the University of Milano with a FEI 20F microscope equipped with an EDS detector, double tilt specimen holder, and a Gatan 794 slow scan CCD. The standardless method was used for semiquantitative microprobe analyses. Crystal aggregates were picked up with a knife blade, dispersed in ethanol, ultrasonicated, and a few drops of suspension were pipetted on holey-carbon copper-grids.

Raman spectra were recorded at the Politecnico di Milano with a LABRAM HR800 employing two laser sources, a solid-state laser (Laser XTRA, Toptica Photonics) operating at 785 nm, and an argon ion laser (Stabilite 2017, Spectra Physics) operating at 514 nm. Either rock fragments without any specific preparation or polished thin sections were used for the experiments.

Automatic electron diffraction tomography (ADT) and further EDS experiments were conducted at the University of Mainz with a TEM FEI-F30 equipped with a Gatan 794 CCD camera and a HAADF detector. The ADT tilt series were collected in STEM mode in steps of 1º with normal parallel illumination and precessing the beam. The PED was performed using the SpinningStar unit developed by NanoMEGAS. A tomographic specimen holder and a cryoholder were used for data collection.

Crystal structure solutions were achieved according to the delta-recycling procedure (Rius 2012). As it is applied to the minerals described in the present study, δ-recycling is basically an iterative difference-Fourier recycling process with coefficients (F_{obs}^2-$\langle F^2 \rangle$) in which the N expected atoms in the unit cell are sought and used for calculating the new phase estimates. Once the model has been found, phases are further refined applying conventional weighted difference Fourier methods (see Rius et al. 2013 for the application of the δ-recycling method to ADT data). Final crystal structure refinements were performed with the least square method as implemented in the SHELX-97 program (Sheldrick 1997). Relevant data collection and refinement information are provided in Table 1. F(*hkl*) list files and the CIF files of the refined structures are provided as supplementary material.

Results

New phase I (hexagonal platelets)

The sample did attract our attention by the presence of white hemispherical aggregates hardly resolvable by a standard optical stereomicroscope and not ascribable by visual inspection to any known mineral species (Fig. 2a). Subsequent SEM-EDS investigations revealed that the spherical aggregates are “hortensia-like” mineral aggregates constituted by numerous pseudohexagonal platelets, up to 20 micron in diameter and few microns in thickness, with perfect basal cleavage (Fig. 2b and 2c). HR-SEM images show that any single platelet is characterized by a strong cleavage and is in fact made of thinner films loosely stacked to each other (Fig. 2d). The EDS spectra only revealed Bi, S and O peaks, indicating a possible Bi sulfate mineral. According to the EDS totals, the H_2O wt% obtained by difference leads to the approximate chemical formula $Bi_2(SO_4)(OH)_4$ (Table 2). Only two Bi sulfate minerals are reported so far, cannonite (Stanley 1992) and riomarinaite (Rögner 2005), but their physical properties as morphology, color, luster, cleavage, etc. did not match our observations[1].

Since the amount of material was not enough for powder XRD measurements and beamtime at appropriate crystallography beamlines capable of handling such small crystals was not available, we

---

[1] During the revision of the present paper a new Bi sulphate, balićžunićite, was approved by the CNMNC (IMA No. 2012-098). The new mineral is triclinic $P\overline{1}$, with cell parameters: a = 6.7386(3), b = 11.1844(5), c = 14.1754(7) Å, α = 80.082(2), β = 88.462(2), γ = 89.517(2)°, and composition $Bi_2O(SO_4)_2$ (Pinto et al. 2013). Balićžunićite structural parameters and composition are diverse than those determined for the new phases found at Alfenza (see ahead).

decided to employ TEM to further characterize the samples. The hexagonal platelets were recognized by their morphology and orientation on the carbon film due to their perfect basal cleavage (Fig. 3a). Selected area electron diffractions revealed a 2*mm* planar symmetry and systematic absences along one of the principal axes (Fig. 3b). The corresponding interplanar distances along principal directions were respectively 17.2(4) and 15.9(3) Å. These crystallographic data combined with the qualitative chemistry could not be attributed to any known mineral phase. Subsequent investigations revealed that this compound also forms massive incrustations covering completely bismuthinite needles (Fig. 4a). In this second type of appearance, single crystals cannot be resolved by BSE images, but locally, where a gradual transition to the well developed pseudohexagonal habit can be recognized (Fig. 4b to c). Moreover, fine scale intergrowths with anglesite and cannonite were detected at the SEM on polished cross sections of bismuthinite needles, and cannonite was unambiguously detected with the TEM.

Raman spectra were acquired on the hortensia-like aggregates of the first type of appearance, where the prevalence of the new phase I is undisputable, using 785 nm and 514 nm laser beams. For the 785 nm radiation, the O-H stretching modes fall at such low energy that they were out of range for the available CCD detector. On the other hand, when using the 514 nm radiation, the interpretation of the O-H stretching region between 3200 and 3500 cm^{-1} is complicated by a significant fluorescence signal. Actually, in that region (Fig. 5, upper), some weak and broad peaks are detected, but as evidenced by the comparison with other hydrated minerals, the O-H stretching modes give sharp and intense peaks when present (e.g., malachite, gypsum, and cannonite), whereas in nominally anhydrous minerals as rhodochrosite there are weak and broad peaks, may be due to superficial adsorbed water or other spurious effects, all similar to those observed in the hortensia-like aggregates. Thus, the Raman investigation cannot confirm the presence of water (*latu senso*) in the new phase I as inferred from the EDS totals, and suggests the possible alternative chemical formula $Bi_2O_2(SO_4)$.

In the lower part of Figure 5, the spectrum of the new phase I is compared with those of other sulfates, namely cannonite, riomarinaite, anglesite, and gypsum in the 0-1300 $\mathrm{cm^{-1}}$ range. The different sulfates can be distinguished by the number of bands and slightly different shifts of the characteristic SO_4 stretching (symmetric and antisymmetric) and bending modes in the 950-1200 and 400-700 $\mathrm{cm^{-1}}$ regions, respectively. That distinction is less palpable for the new phase I and cannonite, which, on the other hand, show very different Bi-O and lattice vibration modes below 330 $\mathrm{cm^{-1}}$.

In order to fulfill the structure characterization of the new phase I, automatic electron diffraction tomography (ADT) experiments were carried out (Mugnaioli et al. 2009; Kolb et al. 2011, and reference therein). Because of the sensitivity of the hexagonal platelets to the electron beam, a tomographic cryoholder to cool the sample down to -180 °C was used. The 3D diffraction data revealed the monoclinic unit cell parameters a = 22.0(4), b = 16.7(3), c = 15.9(3) Å, β = 102.9(2.1)°, with **a*** orthogonal to the basal plane. The reflection conditions $h0l$, $l = 2n$ (Fig. 6, left) are consistent with the extinction symbol $P1c1$, leading to the acentric Pc or the centric $P2/c$ space groups (Table 1). Diffuse scattering along **a*** for all reflections with $l \neq 2n$ and $k \neq 3n$ (Fig. 6, right), suggests for the possible existence of polytypes built up by **c/2** x **b/3** subcells. Because of the complications arising from the two-dimensional stacking disorder and the sensitivity to the beam that resulted into poor quality data (and possibly because of the low symmetry and large cell size), the structure solution failed. We also tried to solve the subcell structure using a halved dataset with only family reflections, but unsuccessfully.

New phase II (crystals with porous structure)

A second bismuth sulfate was detected on the same TEM mounts used for the characterization of the previous mineral and distinguishable at first sight from the latter by the lack of a preferential orientation, e.g. absence of a net cleavage plane. This second bismuth sulfate is also comparatively more stable under the electron beam and has different unit cell dimensions and symmetry. Its EDS spectrum, however, is almost undistinguishable from that of the hexagonal platelets, but for the presence of a small amount of tellurium (Fig. 7 and Table 3). The unit cell of this second phase, as determined by ADT, is hexagonal with $a = 9.5(2)$ and $c = 15.4(3)$ Å. According to the observed systematic absences, the extinction group is $P--c$. Also this second bismuth sulfate has crystallographic and compositional features not shared with any known mineral phase.

The structure solution was achieved by δ-recycling in both space groups $P\overline{6}2c$ and $P31c$. The presence of a mirror plane orthogonal to [001] in the $P31c$ solution confirmed $P\overline{6}2c$ as the true symmetry, which was entered in the definitive δ-recycling runs. Inspection of the best δ-recycling solutions clearly showed that the crystal structure is formed by Bi-S-O units composed by one $Bi_9(OH)_6O_8$ cluster and two sulfate SO_4 tetrahedra (hydrogen was not located on the electron density map but placed on the basis of structural consideration). Every cell contains 2 such Bi-S-O units. EDS analysis shows that the structure also holds a small amount of Te, probably partially replacing Bi. By assuming Te to have oxidation state 4^+, the formula of one Bi-S-O unit is $[Bi_{9-x}Te_x(OH)_6O_8(SO_4)_2]_{1+x}$. The δ-recycling model also shows four additional peaks (assigned to S atoms) along the channel at the origin of the unit cell. They form S-S pairs with interatomic distances of 2.11 Å (Fig. 8). All attempts to introduce O ligands bonded to these S atoms failed. Finally, the S-S pair was assigned to a disulfide anion $(S_2)^{2-}$. According to the average Bi:Te ratio (Table 3), there should be 16.5 Bi atoms and 1.5 Te atoms per cell. In order to compensate the charge, 1.75 $(S_2)^{2-}$ anions should be in the channel, for a total amount of 7.5 S atoms per cell (4 from sulfate groups and 3.5 from disulfide anions). Actually, this number is in good agreement with the EDS estimation of 7.6 S atoms per cell (Bi/S ≈ 2.25, Table 3).

The unit cell content is then given by the general formula $(S_2)_{1+x}[Bi_{9-x}Te_x(OH)_6O_8(SO_4)_2]_2$. For the least-squares refinement of the ADT data with SHELX-97, the Te content used ($x = 0.82$) was derived from a single EDS analysis performed at the same zone where the ADT measurement was carried out. As electron scattering factors for Te are not available in the employed dataset (Doyle and Turner 1968), scattering factors from nieghboring Sb were used instead. The refinement turned out to be stable only assuming all the Te at the Bi1 site. Figures of merit, refined parameters and restraints (2 distance restraints for the S-O bonds of the sulfate group) are reported in Table 1; atomic positions and displacement factors in Table 1s as supplementary material and selected bond distances in Table 4, respectively.

The crystal structure can be described as a self-assemblage of Bi-S-O units making zig-zag chains along [001] and giving rise to a porous material. Both symmetry independent Bi^{3+} have the same coordination, i.e. a pentagonal bipyramid with one Bi-O bond length longer than 3 Å (Table 4). A sketch down the hexagonal axis is given in Figure 8b. From this appealing view, the structure of the new phase II looks like a “bismuth-zeolite” with one dimensional porosity (the diameter of the channel is about 7 Å).

Cannonite

Cannonite is a rare mineral which probably forms from alteration of bismuth sulfides. Although noticed several decades before in Cu-Bi-S mineralization at the Ohio Mining District, Marysvale, Utah (Radtke et al. 1967), it has been reported as a new mineral only in 1992 (Stanley et al. 1992), and its structure is known only from synthetic analogues (Aurivillius 1964; Golič et al. 1982). Cannonite findings have later been reported from a few other localities, but in most cases, with the possible exception of the Duadello Mine finding (Pisogne Valley, Brescia, Italy; Britvin et al. 2003), identification was done by visual inspection or EDS analyses, thus rising doubts about the reliability of the identification, and it is probable that in some cases (e.g. samples from Puy-les-Vignes, Saint-Léonard-de-Noblat, Haute-Vienne, France), the new bismuth sulfate described above with the appearance of “hortensia-like” aggregates were misidentified as cannonite.

At Alfenza, cannonite forms radiating, acicular aggregates of colorless, transparent crystals with “scalpel-like” habit, elongated along **c**, up to 200 micron in length (Fig. 9). The mineral was unambiguously identified through ADT data, yielding cell parameters a = 7.7(2), b = 13.9(3), c = 5.7(1) Å, β = 109.8(5)°, and space group $P2_1/c$. Its chemical composition as obtained from TEM-

EDS analyses is compared in Table 3 with the other bismuth sulfates and sulphides found at Alfenza and its Raman spectrum is reported in Figure 5.

The cannonite structure was successfully solved *ab initio* and refined using electron diffraction data (relevant data collection and refinement data in Table 1). These data, although of not excellent quality, were sufficient to attest the structural identity of this natural sample with the synthetic analogue described by Aurivillius (1964) and Golič et al. (1982). A detailed crystal structure description of cannonite from Alfenza from single crystal X-ray data along with microchemical and spectroscopic data will be reported elsewhere.

Discussion and Conclusions

In general, and as well in the present study, structures solved with electron crystallography show larger residues when compared with similar structures solved through X-ray diffraction data. The reasons have been extensively discussed in literature (e.g., Dorset et al. 2005; Zou et al. 2011) and relay on: i) not fully kinematical conditions; ii) geometry conditions of the data collection – the positioning of the sample in the TEM is not so accurate as in a single crystal diffractometer and the Ewald sphere sampling is usually smaller due to the "missing cone" (Mugnaioli and Kolb 2013) – iii) effective routines for data reduction (absorption and Lorenz corrections) not yet available; iv) beam damage during data acquisition (e.g., Kolb et al. 2010). All these problems affect the diffraction intensity and determine high discrepancy indexes in the final structure refinements. Notwithstanding, there is a large number of reports about successful solutions of structures with electron diffraction data, and in particular with the ADT method, in spite of large residues (e.g. Jiang et al. 2011; Gemmi et al. 2012; Rius et al. 2013). The cannonite structure reported in this study is an additional example of the feasibility of structure solution by electron diffraction data. Thus, whereas electron diffraction still needs improvements in order to achieve residues comparable to XRD analysis, this technique is becoming routinely for *ab initio* structure solution.

The Alfenza Mine is going to be more renowned for the mineralogical variety that it has so far supplied than as a resource for noble metals for the future. As a matter of fact, of the about 7000 tons of auriferous pyrite globally estimated in the Alfenza area, two thirds have already been taken out, and the remaining one virtually still in place apparently has been judged to be not economically remunerative. On the other side, a vast variety of minerals has been reported from Alfenza. A long list has been compiled by Roggiani (1946), to be updated with cosalite and native gold (Roggiani 1970), and, possibly, with the two new bismuth sulfates and a rare one, cannonite, reported in this paper.

The first new mineral (new phase I) forms white, microscopic hexagonal platelets that individually look like mica. Chemical analyses and spectroscopic data are contradictory, since the former indicates a hydroxy bismuth sulfate with formula $Bi_2(SO_4)(OH)_4$, while the latter a Bi oxy-sulfate with formula $Bi_2O_2(SO_4)$. Water is expected in this mineral because of its secondary origin and crystal morphology, recalling micas and other sheet silicates, such as lizardite or talc for instance, where interlayer hydroxyls hold TO or TOT layers together. Since the paucity of the material and the very small crystal size, the only method we have had to measure the water content was from EDS analyses by difference of the oxide sum to 100%. However, it is well known that this method could be highly inaccurate since any experimental error, such as fluctuation in the beam current, sublimation of elements during acquisition, any deviation from a perfect horizontal and polished analyzed surface, is transferred to the oxide wt% totals. As a matter of fact, Raman spectra do not evidence the presence of H_2O (as well as other light molecules, such as CO_2, to which the EDS detector is poorly or not sensitive thus leading to similar low totals) and suggest the $Bi_2O_2(SO_4)$ formula. One possibility is that the mineral originally contained hydroxyls and that it lost its water content after removal from its minerogenic environment, as suggested by HR-SEM images that show incipient parting of (100) planes. A number of other sulfates are known to vary their water content at ambient conditions: melanterite ($FeSO_4{\cdot}7H_2O$) for instance may dehydrate to siderotil ($FeSO_4{\cdot}5H_2O$); similarly, epsomite ($MgSO_4{\cdot}7H_2O$) may transform to hexahydrite ($MgSO_4{\cdot}6H_2O$). The second bismuth sulfate, also a new phase (new phase II) that occurs at Alfenza, could not be observed in its integral microscopic appearance, since it has been detected repeatedly, but only as crystal fragments at the TEM (Fig. 7). Therefore, even if the occurrence and the composition of the phase II clearly point to the fact that it belongs to the same mineral environment of bismuthinite, i.e. cannonite, and the hexagonal platelets described above (new phase I), we do not know its microscopic appearance, i.e. crystal habit and growth relationships with the other phases. Since it has been found along with the hexagonal platelets from hemispherical aggregates of the first type of appearance, we suppose that the “zeolite-like” phase forms a minor phase intergrown with the former bismuth sulfate. From these fragments, however, we were able to solve the structure and observe its interesting one-dimensional porosity, recalling silicate minerals of the zeolite group. The crystal structure refinement of the zeolite-like structure indicates disulfide anions as the most probable molecular group within the channels.

A third mineral, cannonite, in this case a rare oxy hydroxi bismuth sulfate, was also found at Alfenza. The two new phases above and cannonite are found within the same centimeter sized hand specimens, often within the same millimeter sized cavities, and possibly form micrometer scale intergrowths. These bismuth sulfates most probably result from the oxidation of bismuthinite, which represent their growth substrate. They occur within quartz dikes along with a number of other minerals, including pyrite, anglesite and micas. Raman spectra indicate locally also the presence of metallic sulfur, and microprobe analyses show the sporadic presence of cosalite. It seems thus that sulfur occurs in a number of different oxidation states within the same millimeter sized area, indicating highly variable oxygen fugacity conditions during the minerogenesis. This situation is not infrequent in superficial hydrothermal deposits and skarns (e.g., Capitani and Mellini 2000).

One of the questions this study raises is about how many new minerals are still in hiding in a rock sample that can be disclosed only with techniques able to investigate at a submicrometer scale. In this work, one new bismuth sulfate in form of hexagonal platelets was disclosed at the SEM, and there is more than an impression that it could be misidentified in the past. A second new bismuth sulfate with a porous structure recalling the silicate zeolites has been observed only with the help of a TEM. The two new phases, along with cannonite, have been characterized with automatic electron diffraction tomography (ADT), a very promising technique that has already been used for the characterization of nanocrystalline minerals (Rozhdestvenskaya et al. 2010, 2011; Gemmi et al. 2011, 2012; Mugnaioli et al. 2012) and most probably will contribute to enlarge the mineralogy database in the future.

An interesting possible somewhat speculative implication of our results concerns the systematics of Bi-sulfates: We solved the structure of a new bismuth sulfate (new phase II) built up of Bi oxide polyhedra connecting into a 3D framework that is reminiscent of a silicate zeolite structure. We found another bismuth sulfate (new phase I), that shows a crystal habit and a structural disorder that mimic micas, a sheet silicate. These two new phases are associated with another bismuth sulfate, cannonite, whose structure consists of infinite chains of irregular bismuth oxide polyhedra running along **c**, similar to inosilicates. Riomarinaite, the other known bismuth sulfate (Grunar et al 1982), not detected in this study, forms pairs of isolated bismuth polyhedra, analogue to di-silicates. In all these minerals, bismuth oxide polyhedra are the basic building unit of the structure, since the sulfate is never polymerized. The interesting question thus is whether or not there is a systematic analogue to silicates for bismuth sulfates? The answer is complicated because, unlike in silicates, Bi-oxide polyhedral units are more varied than the ubiquitous SiO_4 tetrahedron and can thus act in a variety of different ways as a complex anion. The opening of the nanoscopic world with the new techniques employed in this study will probably help finding an answer to this question.

Acknowledgements

Vittorio Mattioli and Claudio Albertini are warmly acknowledged. Vittorio because his curiosity pushed us to investigate the Alfenza samples he provided, discovering the very fascinating microscopic word described in this paper. Claudio for introducing us into the historical background of the Alfenza Mine and providing the related literature material. We are indebted with Robert Branscheid (University of Mainz) for his excellent work at the HR-SEM. ADT has been supported by the Stiftung Rheinland-Pfalz für Innovation. Comments by the Associated Editors, Oliver Tschauner and Martin Kunz, two anonymous referees and the technical editor greatly improved the manuscript. This paper is in memory of Lileo Capitani.

References

Aurivillius, B. (1964) The crystal structures of $Bi_2O_2SO_4 \cdot H_2O$ and $BiOHSeO_4 \cdot H_2O$. Acta Chemica Scandinavica,18, 2375-2378.

Avilov, A., Kuligin, K., Nicolopoulos, S., Nickolskiy, M., Boulahya, K., Portillo, J., Lepeshov, G., Sobolev, B., Collette, J.P., Martin, N., Robins, A.C., Fischione, P. (2007) Precession technique and electron diffractometry as new tools for crystal structure analysis and chemical bonding determination. Ultramicroscopy, 107, 431-444.

Bianchi, A. (1924) - La bismutinite di Crodo, in Val d'Ossola e le costanti cristallografiche della bismutinite. Rendiconti della Reale Accademia dei Lincei, XXXIII, 254-258.

Britvin, S., Sturla, M., Bonacina, E., Zambetti, L., 2003. Nuovi minerali della miniera del Duadello (Val Pisogne, Brescia). Rivista Mineralogica Italiana, 27 (2), 107-108.

Capitani, G.C., Mellini, M. (2000) The crystallisation sequence of the Campiglia M.ma skarn (Livorno, central Italy). Neues Jahrbuch fur Mineralogie – Monatshefte, 3, 97-115.

Dorset, D.L., Roth, W.J., Gilmore, C.J. (2005) Electron crystallography of zeolites – the MWW family as a test of direct 3D structure determination. Acta Crystallographica, A61, 516-527.

Doyle, P.A., Turner, P.S. (1968) Relativistic Hartree-Foek X-ray and Electron Scattering Factors. Acta Crystallographica, A24, 390-397.

Ferraris, G., Franchini, A.M., Roggiani, A.G. (1970) Cosalite nelle miniere aurifere del torrente Alfenza (Crodo, Valle d'Ossola). Periodico di Mineralogia, XXXIX, 1, 165-172.

Gemmi, M., Campostrini, I., Demartin, F., Gorelik, T.E., Gramaccioli, C.M., (2012) Structure of the new mineral sarrabusite, $Pb_5CuCl_4(SeO_3)_4$, solved by manual electron diffraction tomography. Acta Crystallographica, B, 68, 15-23.

Gemmi, M., Fischer, J., Merlini, M., Poli, S., Fumagalli, P., Mugnaioli, E., Kolb, U., (2011) A new hydrous Al-bearing pyroxene as a water carrier in subduction zones. Earth Planetary Science Letters, 310, 422-428.

Golič, L., Graunar, M., Lazarini, F. (1982) Catena-Di-μ-hydroxo-μ3-oxo-dibismuth(III) Sul fate. Acta Crystallographica, B38, 2881-2883.

Graunar, M., Lazarini, F. (1982) Di-μ-hydroxo-bis[aquasulfatobismuth(lll)]. Acta Crystallographica, B38, 2879-2881.

Jiang, J., Jorda, J.L., Yu, J., Baumes, L.A., Mugnaioli, E., Diaz-Cabanas, M.J., Kolb, U., Corma, A. (2011) Synthesis and structure determination of the hierarchical meso-microporous zeolite ITQ-43. Science, 333, 1131-1134.

Kolb, U., Gorelik, T.E., Kübel, C., Otten, M.T., Hubert, D. (2007) Towards automated diffraction tomography: Part I—Data acquisition. Ultramicroscopy, 107, 507-513.

Kolb, U., Gorelik, T.E., Mugnaioli, E., Stewart A. (2010) Structural characterization of organics using manual and automated electron diffraction. Polymer Reviews, 50, 385-409.

Kolb, U., Mugnaioli, E., Gorelik, T.E. (2011) Automated electron diffraction tomography – a new tool for nano crystal structure analysis. Crystal Research and Technology, 46, 542-554.

Mugnaioli, E., Andrusenko, I., Schüler, T., Loges, N., Dinnebier, R.E., Panthöfer, M., Tremel, W., Kolb, U. (2012) Ab Initio Structure Determination of Vaterite by Automated Electron Diffraction. Angewandte Chemie International Edition, 51, 7041-7045.

Mugnaioli, E., Gorelik, T., Kolb, U. (2009) “Ab initio” structure solution from electron diffraction data obtained by a combination of automated diffraction tomography and precession technique. Ultramicroscopy, 109, 758-765.

Mugnaioli, E., Kolb, U. (2013) Applications of automated diffraction tomography (ADT) on nanocrystalline porous materials. Microporous and Mesoporous Materials, 166, 93-101.

Pinto, D., Garavelli, A. Mitolo, D. (2013) Balićžunićite, IMA 2012-098. CNMNC Newsletter No. 16, August 2013, page 2699; Mineralogical Magazine, 77, 2695-2709.

Pipino, G. (2003) Oro, Miniere, Storia. Miscellanea di giacimentologia e storia mineraria Italiana. Ed. Museo Storico dell’Oro Italiano, Ovada, 510 pp.

Radtke, A.S., Taylor, C.M., Frost, J.E. (1967) Bismuth and tin minerals in gold- and silver-bearing sulphide ores, Ohio Mining District, Marysvale, Utah. U.S. Geological Survey Professional Paper, 575-D, D127-30.

Rius, J. (2012) Direct phasing from Patterson syntheses by δ recycling. Acta Crystallographica, A68, 77–81.

Rius, J., Mugnaioli, E., Vallcorba O., Kolb, U. (2013) Application of δ recycling to electron automated diffraction tomography data from inorganic crystalline nanovolumes. Acta Crystallographica, A69, 396–407.

Roggiani, A.G. (1940) Il regno minerale nell'Ossola. II° La bismutinite delle miniere aurifere di Crodo "Secondo ritrovamento". Tipografia C. Antonioli, Domodossola, 11 pp.

Roggiani, A.G. (1946) Il regno minerale nell'Ossola. V° Le miniere aurifere del torrente Alfenza (Crodo) "Elenco dei Minerali". Tipografia C. Antonioli, Domodossola, 30 pp.

Roggiani, A.G. (1948) Appunti per una descrizione della miniera aurifera dell'Alfenza in territorio di Crodo in Val d'Ossola. Natura, XXXIX, 1, 9-21.

Roggiani, A.G. (1970) Appunti per una mineralogia dell'Ossola: Oro nativo e cosalite: due ulteriori conferme sulla validità scientifica dei giacimenti auriferi dell'Alfenza (Crodo). Illustrazione Ossolana, XII, 4, 104-112.

Rögner, P. (2005) Riomarinaite, a new bismuth mineral from Falcacci stope, Rio Marina, Elba (Italy). Der Aufschluss, 56, 53-60 (in German with English abstract).

Rozhdestvenskaya, I., Mugnaioli, E., Czank, M., Depmeier, W., Kolb, U., Reinholdt, A., Weirich, T. (2010) The structure of charoite, $(K,Sr,Ba,Mn)_{15-16}(Ca,Na)_{32}[(Si_{70}(O,OH)_{180})](OH,F)_{4.0}*nH_2O$, solved by conventional and automated electron diffraction. Mineralogical Magazine, 74, 159-177.

Rozhdestvenskaya, I., Mugnaioli, E., Czank, M., Depmeier, W., Kolb, U., Merlino S. (2011) Essential features of the polytypic charoite-96 structure compared to charoite-90. Mineralogical Magazine, 75, 2833-2846.

Sheldrick, G.M. (1997) SHELXL-97, A program for crystal structure refinement. University of Göttigen, Germany, release 97-2.

Stanley, C.J., Roberts, A. C., Harris, D. C., Criddle, A. J., Szymaińsky, J.T. (1992) Cannonite, $Bi_2O(OH)_2SO_4$, a new mineral from Marysvale, Utah, USA. Mineralogical Magazine, 56, 605-609.

Stella, A. (1943) I giacimenti auriferi delle Alpi Italiane. Memorie descrittive della Carta Geologica d'Italia, 27.

Vincent, R., Midgley, P. A., (1994) Double conical beam-rocking system for measurement of integrated electron diffraction intensities. Ultramicroscopy, 53, 271-282.

Zou, X., Hovmöller, S., Oleynikov, P. (2011) Electron Crystallography: Electron Microscopy and Electron Diffraction. Oxford Science Publications.

Caption to figures

Figure 1. Reproduction of the original geological map of the Crodo Area as compiled by Stella (1943). White: quaternary tillitic and alluvium deposits; dots: Jurassic calceschists and phyllites; black: Triassic mudstones; dashes: early Triassic garnet micaschists; horizontal lines: pre-Triassic

orthogneiss. NNW-SSE parallel marks between Crodo and Viceno represent the mineralized quartz dikes.

Figure 2. (a) Optical stereo-micrograph of hemispherical (hortensia-like) crystal aggregates of the new hydroxy bismuth sulfate (white) described in this work (new phase I), which grows on bismuthinite (dark), which in turn is embedded in quartz (grey). (b) and (c) SEM-BSE images of the hortensia-like aggregates. The pseudo-hexagonal flat habit of each crystallite is well visible. (d) HR-SEM image of the pseudo-hexagonal platelets. Note the incipient parting of the basal planes, possibly related to stacking disorder.

Figure 3. (a) BF-TEM image of hexagonal platelets dispersed on holey carbon film. The pseudo-hexagonal morphology observed at the SEM can be recognized. (b) SAED pattern taken on the uppermost side of the largest platelet. Note the 2*mm* plane symmetry and the systematic absences along the sub-horizontal main axis.

Figure 4. (a) Optical stereo-micrograph of prismatic crystals of bismuthinite entirely covered by bismuth sulfate. (b) SEM-BSE image of the same V-shaped crystals imaged in (a). (c) Close up of the V-shaped region with bismuth sulfate massive incrustation (top left), subhedral platelets, and sheet silicates (dark, right). The latter can also be recognized in (a). (d) Heuedral, well crystallized platelets.

Figure 5. (Upper) Micro-Raman spectra of the hexagonal platelets (new phase I) as compared with other hydrated (gypsum, $CaSO_4 \cdot 2H_2O$; malachite, $Cu_2(CO_3)(OH)_2$; cannonite, $Bi_2O(SO_4)(OH)_2$) and anhydrous (rhodochrosite, $MnCO_3$), minerals in the 50-1800 cm^{-1} range (left) and in the 3000-3800 cm^{-1} range (right). (Lower) Comparison between the Raman spectrum of the hexagonal platelets (new phase I) with other sulfates relevant for this study in the 50-1300 cm^{-1} range. All the spectra were acquired during this study, except riomarinaite [$Bi_2O(SO_4)(OH)_2$] and anglesite ($PbSO_4$), that come from the RRUFF database.

Figure 6. Three dimensional reciprocal lattice of the hexagonal platelets (new phase I) as seen down [100] (left), [010] (upper right), and [001] (lower right). Major disorder, evidenced by streaks along

a*, is detected for *hkl*, $l \neq 2n$ (upper right), and *hkl*, $k \neq 3n$ (lower right). Streaks are normal to the basal surface and possible direction of stacking of the platelets, and cannot be seen along [100] (left). Relative good order is observed for all the other reflections (large arrows). Note: the apparent curvature of the reciprocal lattice rows in [010] and [001] projections is due to *z*-drift of the cryoholder during the tilt series acquisition of the reciprocal lattice slices.

Figure 7. (a) STEM image of a crystal fragment of the new phase II that was used for structure solution (smaller, rectangular crystal on the lower right) and (b) related EDS spectrum with the most intense fluorescence peaks labeled. Note the doublet (K_α and K_β) peaks of Te at ~3.80-4.10 keV. The S_K peak is hardly visible as a bump on the left side of the Bi_M_α peak. The Fe_K peaks come from the objective pole pieces and the Cu peaks from the TEM grid.

Figure 8. Structural sketch of the bismuth sulfate with the “zeolite-like” structure (new phase II) found at Alfenza. (a) Projection down the [010] axis (purple: Bi atoms; red: oxygen atoms; pink; hydroxyls; yellow: $(SO_4)^{2-}$ and $(S_2)^{2-}$ groups). Note the zig-zag chains along [001] of $Bi_9(OH)_6O_8$ modules cemented by SO_4 tetrahedra. (b) Projection down the [001] axis. Note the presence of channels with a diameter of ~7 Å filled with disulfide anions.

Figure 9. (a) and (c) stereo-micrographs of fan-shaped aggregates of cannonite on bismuthinite crystals; (b) and (d): corresponding SEM-BSE images. Note the scalpel-like habit of the crystals.

Table 1. Electron diffraction structural data and refinement parameters of bismuth sulfates from the Alfenza Mine.

	New phase I	**New phase II**	**Cannonite**
a (Å)	22.0(4)	9.5(2)	7.7(2)
b (Å)	16.7(3)	9.5(2)	13.9(3)
c (Å)	15.9(3)	15.4(3)	5.7(1)
α (°)	90	90	90
β (°)	102.9(5)	90	109.8(5)
γ (°)	90	120	90
V (Å^3)	5694(181)	1204(43)	574(22)
Space group	Pc or $P2/c$	$P\bar{6}2c$	$P2_1/c$
Crystal size (µm)*	1.1x1.0x0.1	0.24x0.14x0.1	0.4x0.3x0.05
Wavelength of radiation (Å)	0.0197	0.0197	0.0197
$(\sin\theta/\lambda)_{max}$ (Å^{-1})	0.42	0.50	0.66
Unique reflections	2098	452	317
R_{eqv} (%)	19.56	23.57	19.11
Range of h, k, l	$-13 < h < 13$	$-9 < h < 9$	$-7 < h < 7$
	$-13 < k < 13$	$-8 < k < 8$	$-9 < k < 10$
	$-13 < l < 13$	$-15 < l < 15$	$-5 < l < 5$
$R(4\sigma)$ (%)	-	21.69	29.80
R_{all} (%)	-	23.76	31.64
GooF	-	1.795	3.196
Reflections with $I > 4\sigma$	-	332	262
Least-squares parameters	-	34	41
Weighting scheme**	-	$w = 1/[(\sigma^2 \cdot F_{obs}^2)+(0.1 \cdot P)]$	$w = 1/[(\sigma^2 \cdot F_{obs}^2)+(0.1 \cdot P)]$

* Crystal thickness was estimated on the bases of TEM images at high tilt. ** $P = (F_{obs}^2 + 2F_{calc}^2)/3$.

F(*hkl*) list files and the CIF files for the new phase II and cannonite are provided as supplementary material.

Table 2. SEM-EDS analyses for the new phase I (hexagonal platelets) found at Alfenza along with literature data on cannonite (Stanley et al. 1992) and riomarinaite (Rögner 2005).

Wt%	**New phase I***	**Cannonite**	**Riomarinaite**
SO_3	13.66 (1.62)	14.18	24.28
Bi_2O_3	80.76 (2.00)	82.53	68.86
Total	94.43 (1.38)	96.71	93.14
H_2O by dif	5.57	3.29	6.86
At%			
S	6.93 (0.98)	8.27	9.80
Bi	14.11 (1.50)	16.54	9.55
H	24.68 (4.27)	17.05	24.61
O	54.29 (2.22)	58.14	56.04
A.f.u.			
S	1.02 (0.11)	1.00	1.05
Bi	2.08 (0.17)	1.99	1.02
H	3.66 (0.76)	2.05	2.64
O	8.00	7.00	6.00
Empirical	$Bi_{2.08}S_{1.01}H_{3.66}O_8$	$Bi_{1.99}S_{1.00}H_{2.05}O_7$	$Bi_{1.02}S_{1.05}H_{2.64}O_6$
Ideal	$Bi_2(SO_4)(OH)_4$	$Bi_2O(SO_4)(OH)_2$	$BiSO_4(OH)\cdot H_2O$

*Average of 13 spot analyses; numbers between brackets refer to the standard deviation.

Table 3. TEM-EDS analyses (cation %) of the bismuth sulfates found at Alfenza and bismuthinite, for comparison.

	1		**2**		**3**		**4**	
S(K)	30.76	(5.30)	29.75	(6.19)	32.68	(0.45)	56.54	(1.11)
Te(L)	-		5.79	(2.93)	-		-	
Bi(L)	69.24	(5.30)	64.46	(7.68)	67.32	(2.72)	43.46	(3.64)
Bi/S	2.25		2.17		2.06		0.77	

1: new phase I (hexagonal platelets); 2: new phase II (zeolite-like structure). (Average of 16 and 4 spot analyses, respectively; numbers between brackets refer to standard deviation). 3: cannonite (single spot); 4: bismuthinite (average of two analyses; numbers between brackets refer to instrumental uncertainty).

Table 4. Selected Bond distances for the new phase II found at the Alfenza Mine.

Bi1-O4	2.09(9)	Bi2-O3	2.14(1)	S1-O1	1.42(2)
Bi1-O5	2.15(7)	Bi2-O5	2.19(4)	S1-O2	1.47(2) x3
Bi1-OH	2.72(7) x2	Bi2-O4	2.29(5)		
Bi1-O1	2.91(2) x2	Bi2-OH	2.44(6)	S2-S2	2.11(9)
Bi1-O5	3.28(9)	Bi2-O2	2.61(4)		
		Bi2-OH	2.74(6)		
		Bi2-O2	3.33(5)		

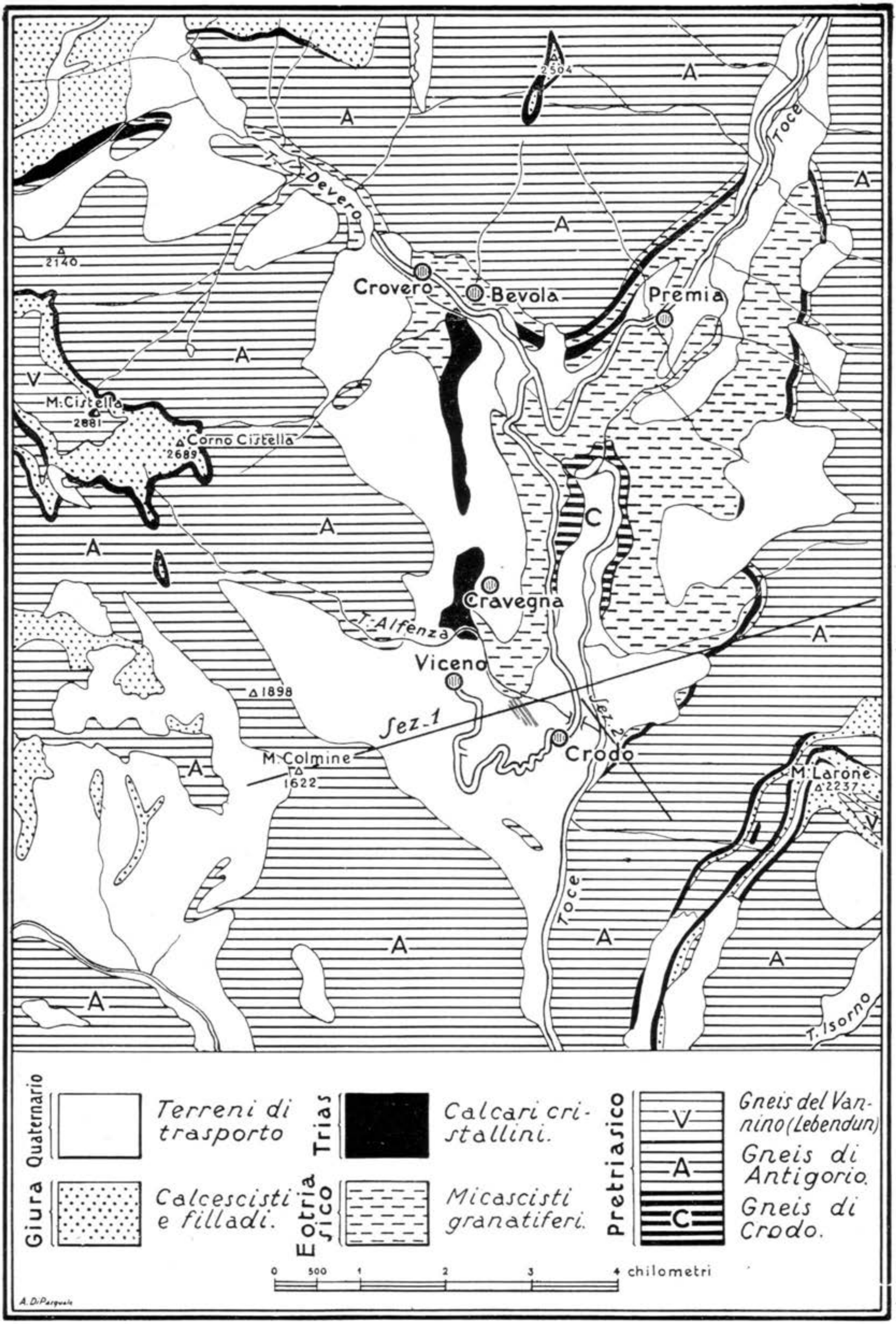
2504
A
Toce
T. Devero
A
2140
Crovero
Bevola
Premia
A
V
M. Cistella
2881
Corno Cistella
2689
A
A
C
Cravegna
T. Alfenza
A
Viceno
1898
Sez. 1
Sez. 2
M. Colmine
1622
A
Crodo
M. Larone
2237
V
Toce
A
A
A
A
T. Isorno
Quaternario
Terreni di trasporto
Giura
Calcescisti e filladi.
Trias
Calcari cristallini.
Eotriasico
Micascisti granatiferi.
Pretriasico
V
Gneis del Vannino (Lebendun)
A
Gneis di Antigorio.
C
Gneis di Crodo.
0
500
1
2
3
4 chilometri
A. Di Pasquale

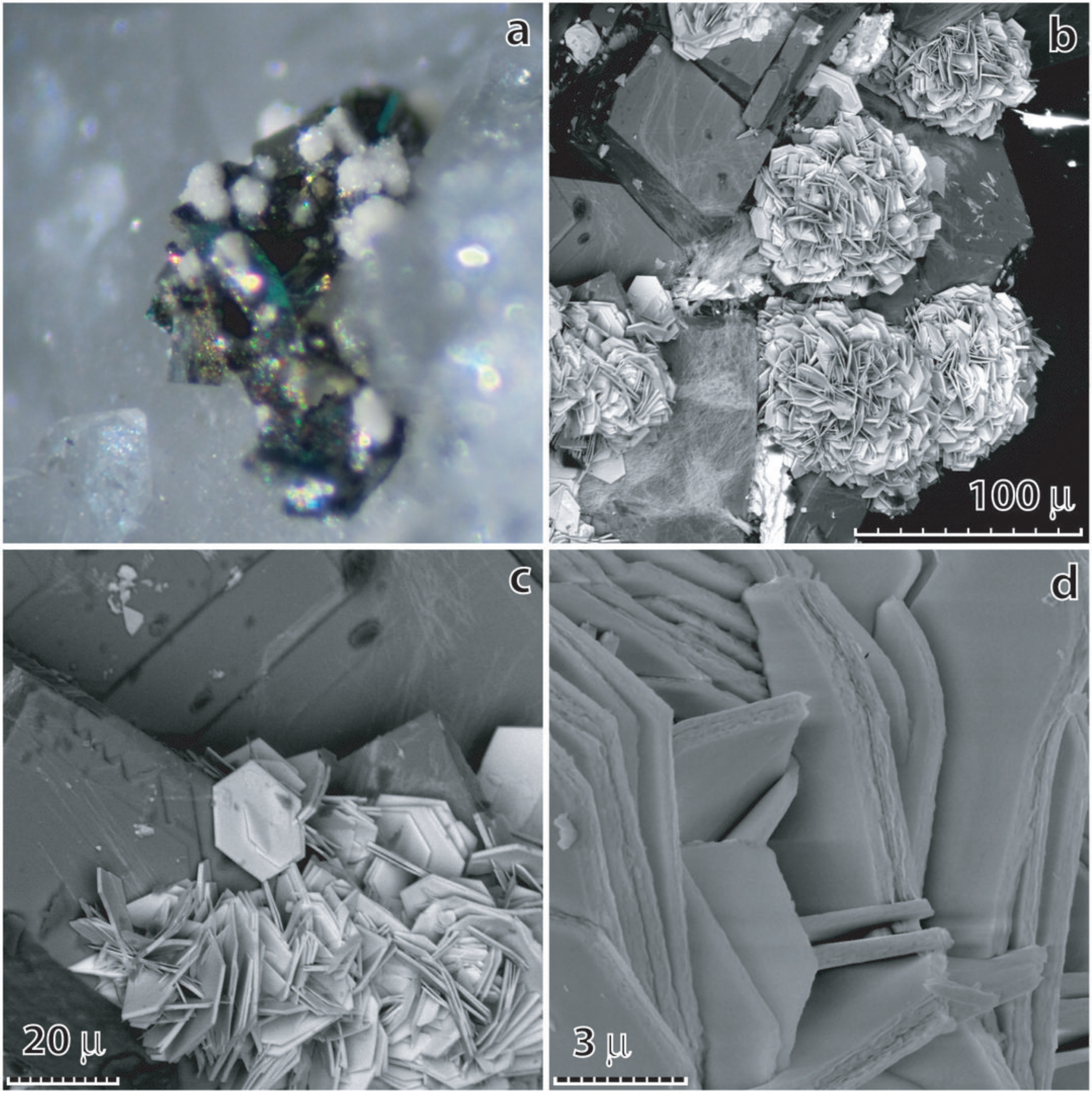
a
b
100 µ
c
20 µ
d
3 µ

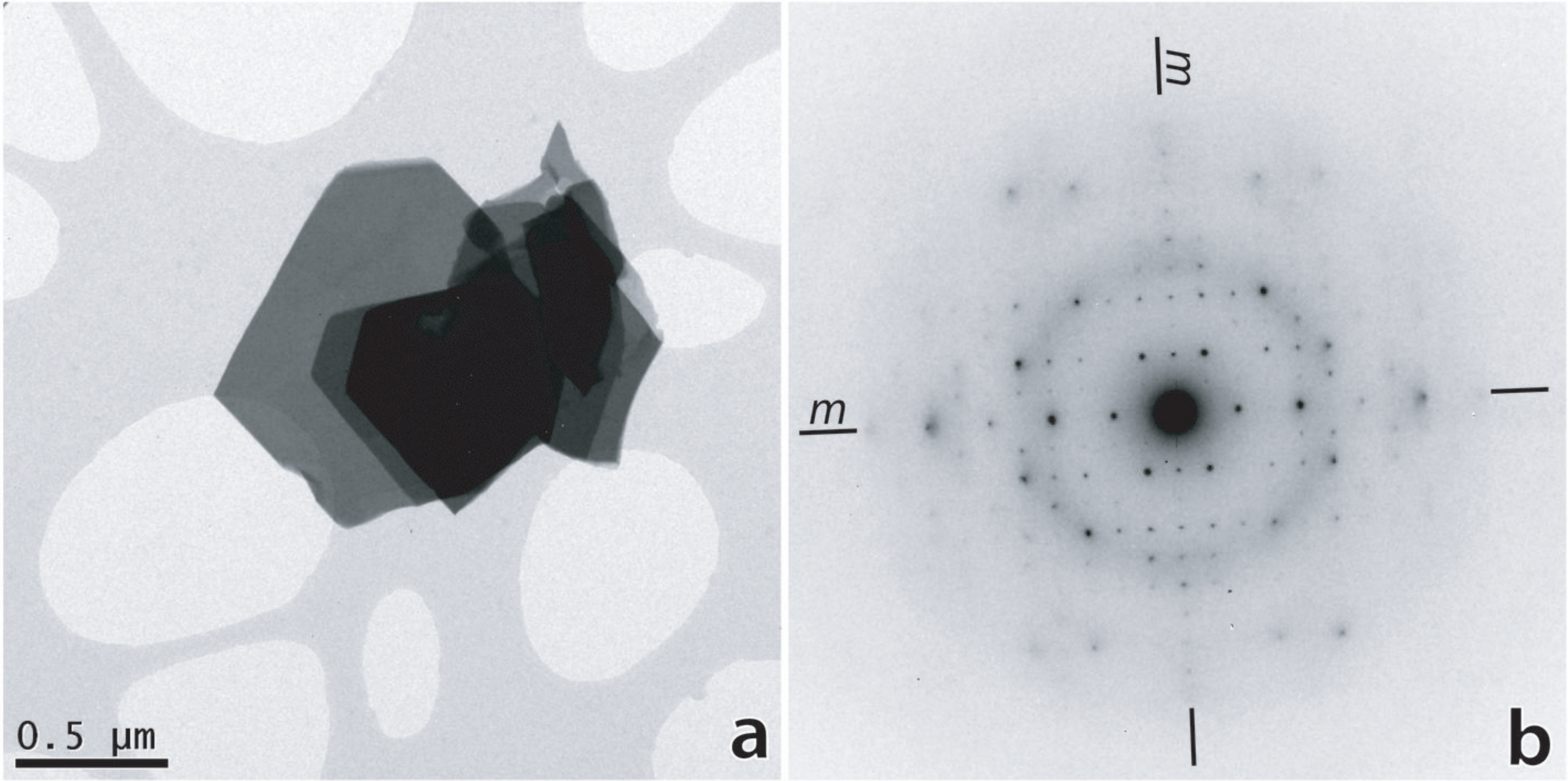
0.5 µm
a
m
m
b

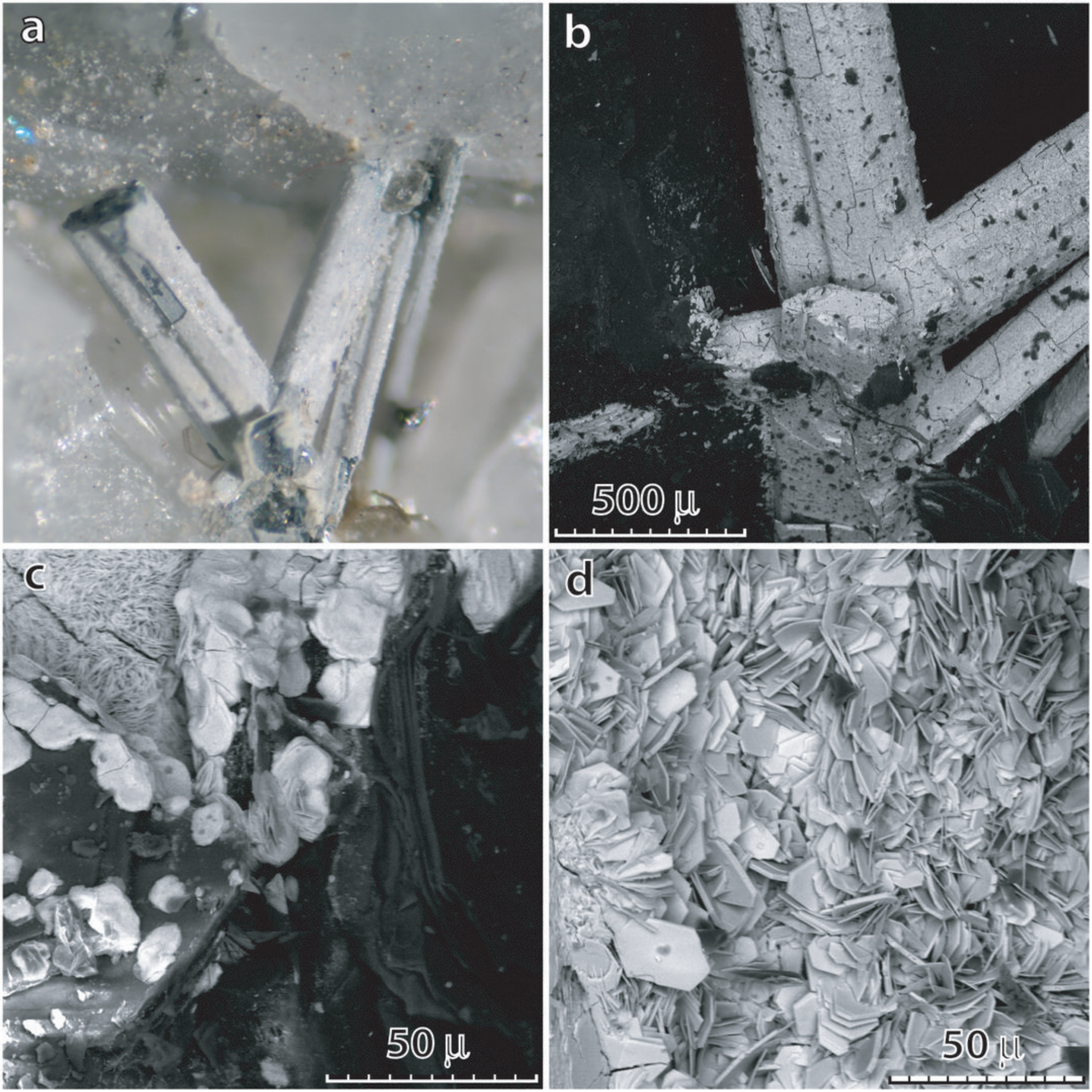
a
b
500 µ
c
50 µ
d
50 µ

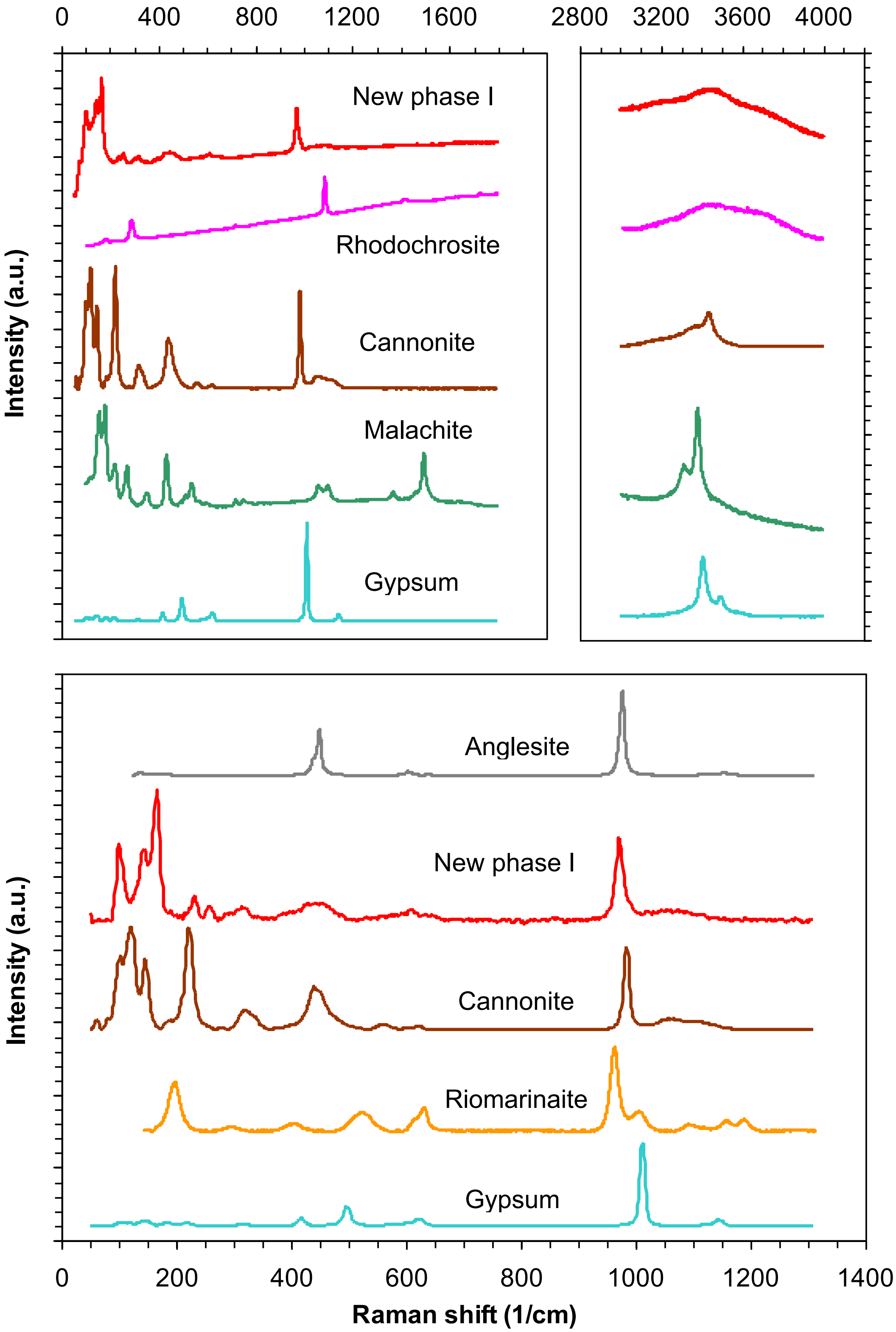
0
400
800
1200
1600
2800
3200
3600
4000
New phase I
Rhodochrosite
Cannonite
Malachite
Gypsum
Intensity (a.u.)
Anglesite
New phase I
Cannonite
Riomarinaite
Gypsum
Intensity (a.u.)
0
200
400
600
800
1000
1200
1400
Raman shift (1/cm)

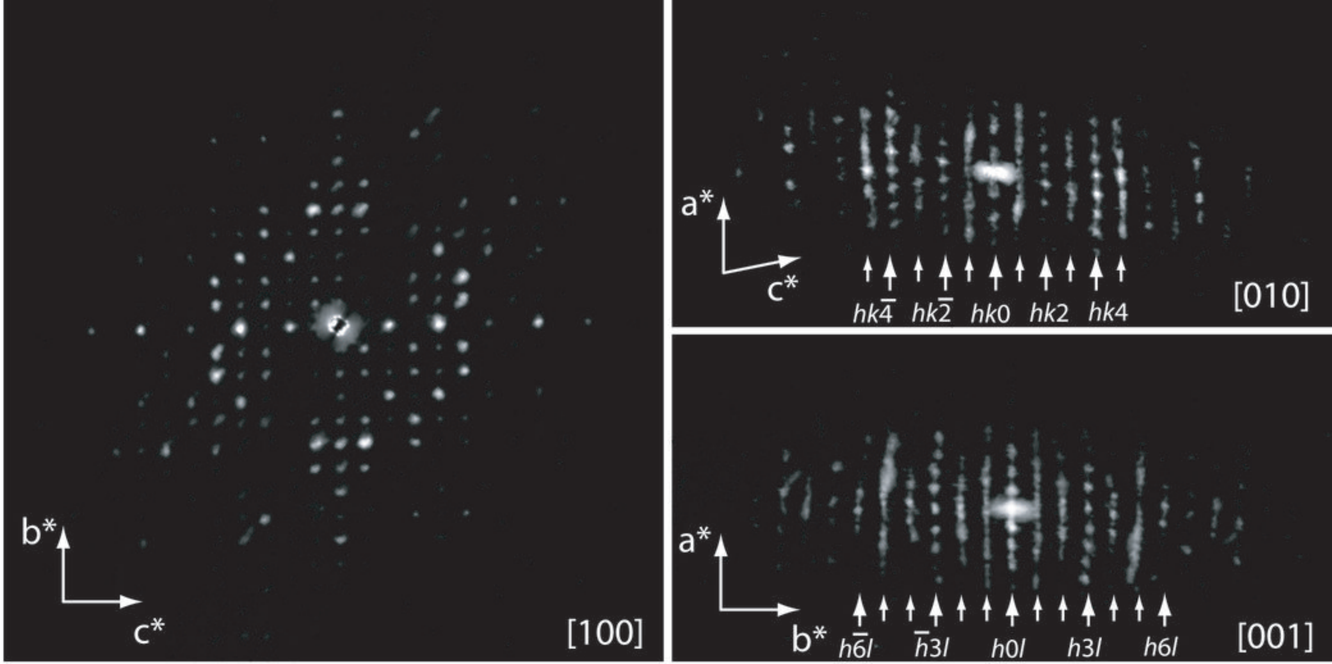
b*
c*
[100]
a*
c*
hk$\bar{4}$
hk$\bar{2}$
hk0
hk2
hk4
[010]
a*
b*
h$\bar{6}$l
$\bar{h}$3l
h0l
h3l
h6l
[001]

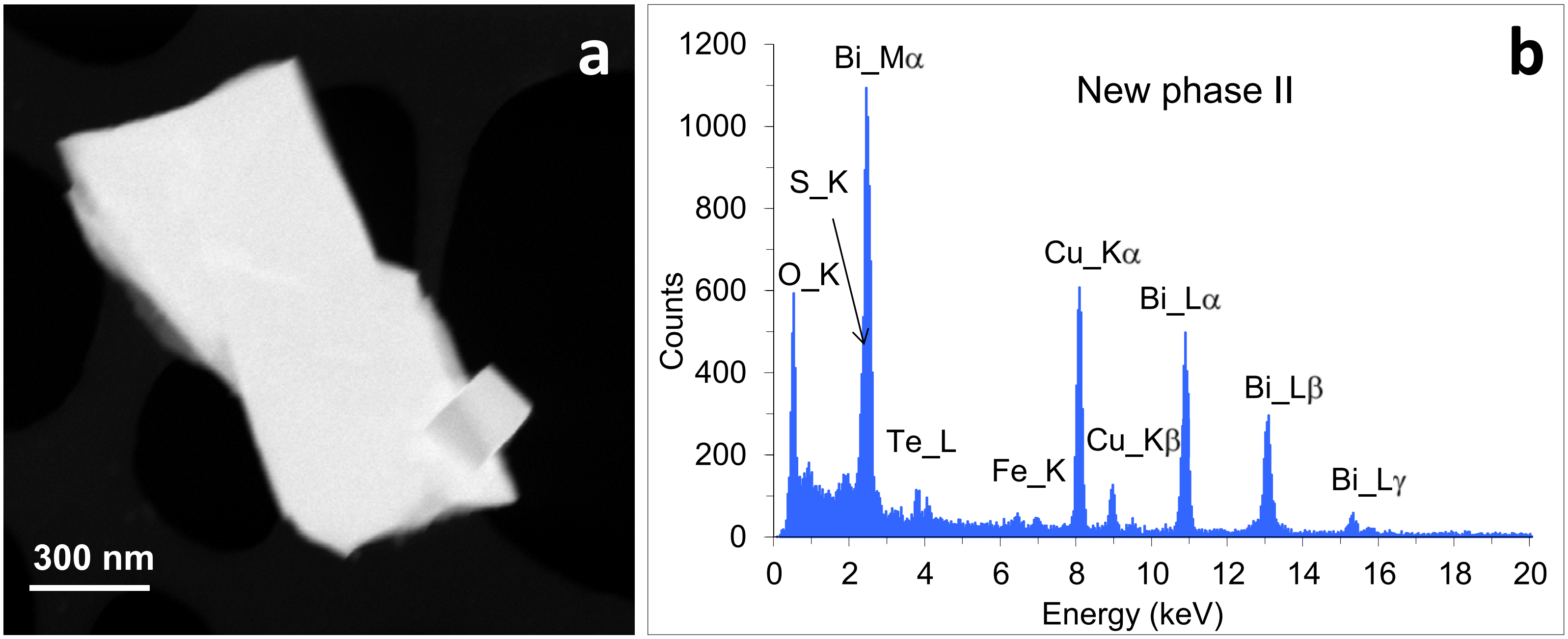
a
300 nm
b
New phase II
Counts
0
200
400
600
800
1000
1200
Energy (keV)
0
2
4
6
8
10
12
14
16
18
20
Bi_Mα
S_K
O_K
Te_L
Fe_K
Cu_Kα
Cu_Kβ
Bi_Lα
Bi_Lβ
Bi_Lγ

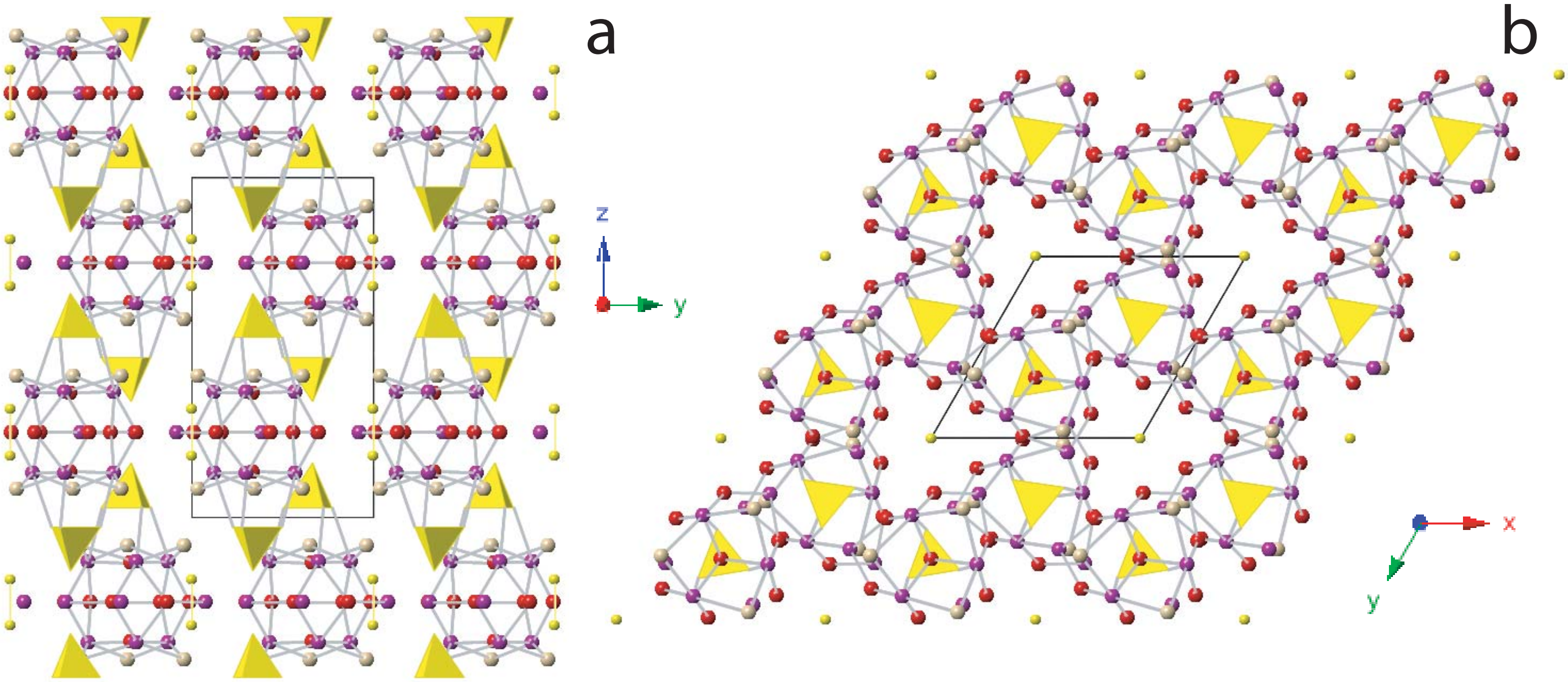
a
z
y
b
x
y

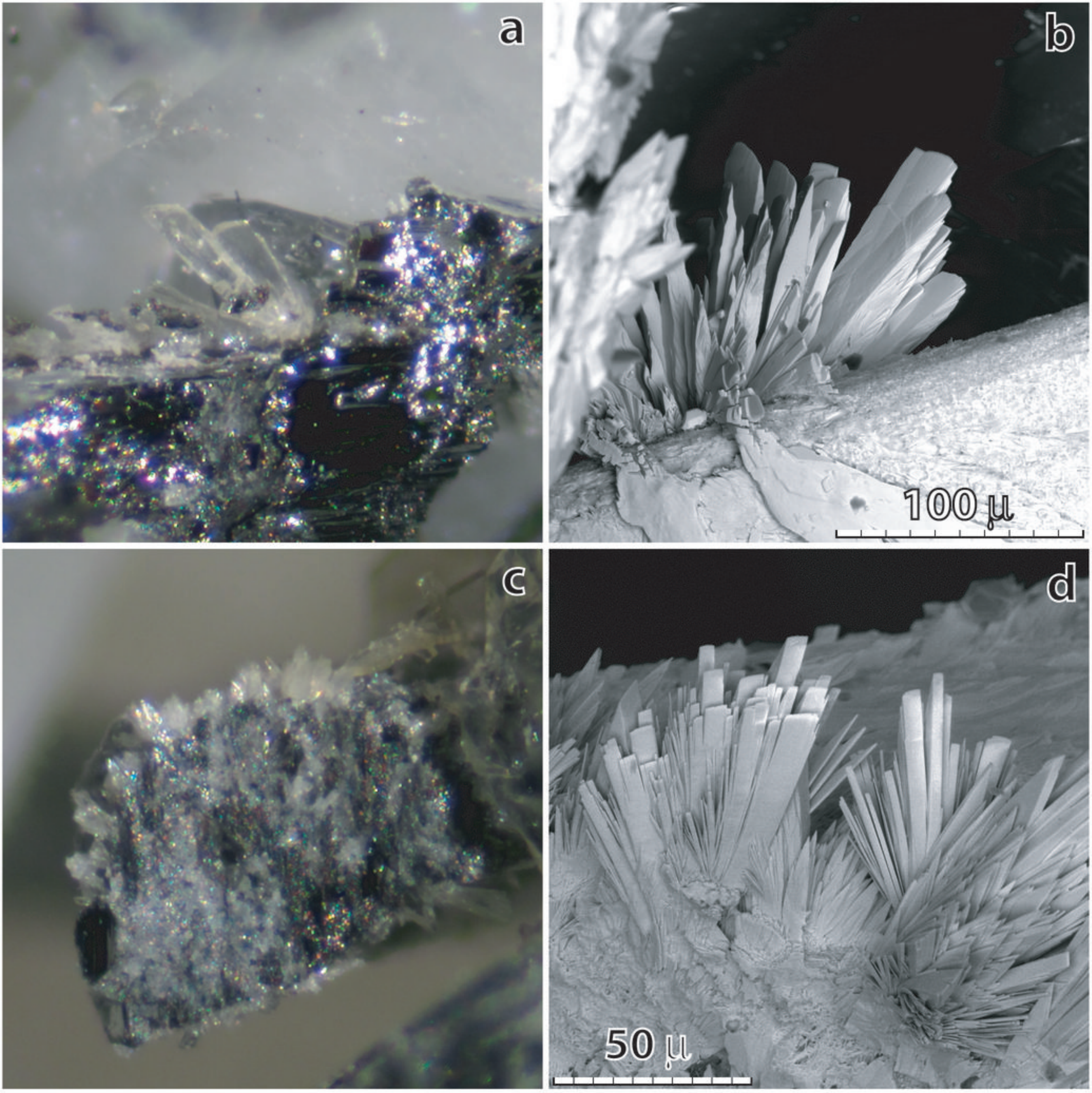
a
b
100 μ
c
d
50 μ